

**OPEN ACCESS**

# Influence of $\text{Al}_2\text{O}_3$ Coatings on HF Induced Transition Metal Dissolution from Lithium-Ion Cathodes

To cite this article: Yonas Tesfamhret *et al* 2022 *J. Electrochem. Soc.* **169** 010530

View the [article online](#) for updates and enhancements.



The Electrochemical Society  
Advancing solid state & electrochemical science & technology

242nd ECS Meeting

Oct 9 – 13, 2022 • Atlanta, GA, US

Abstract submission deadline: **April 8, 2022**

Connect. Engage. Champion. Empower. Accelerate.

**MOVE SCIENCE FORWARD**



Submit your abstract





# Influence of Al<sub>2</sub>O<sub>3</sub> Coatings on HF Induced Transition Metal Dissolution from Lithium-Ion Cathodes

Yonas Tesfamhret,<sup>z</sup>  Reza Younesi,<sup>ib</sup>  and Erik J. Berg<sup>z</sup> 

Department of Chemistry-Ångström Laboratory, Uppsala University, Box 538, SE-75121 Uppsala, Sweden

Transition metal (TM) dissolution from oxide cathode materials is a major challenge limiting the performance of modern Li-ion batteries. Coating the cathode materials with thin protective layers has proved to be a successful strategy to prolong their lifetime. Yet, there is a lack of fundamental understanding of the working mechanisms of the coating. Herein, the effect of the most commonly employed coating material, Al<sub>2</sub>O<sub>3</sub>, on suppressing hydrofluoric acid(HF)-induced TM dissolution from two state-of-the-art cathode materials, LiMn<sub>2</sub>O<sub>4</sub> and LiNi<sub>0.8</sub>Mn<sub>0.1</sub>Co<sub>0.1</sub>O<sub>2</sub>, is investigated. Karl Fischer titration, fluoride selective probe and inductively coupled plasma optical emission spectrometry are coupled to determine the evolution of H<sub>2</sub>O, HF and TM concentrations, respectively, when the active materials come in contact with the aged electrolyte. The coating reduces the extent of TM dissolution, in part due to the ability of Al<sub>2</sub>O<sub>3</sub> to scavenge HF and reduce the acidity of the electrolyte. Delithiation of the cathode materials, however, increases the extent of TM dissolution, likely because of the higher vulnerability of surface TMs in +IV oxidation state towards HF attack. In conclusion, the current study evidences the important role of acid-base reactions in governing TM dissolution in Li-ion batteries and shows that coatings enhance the chemical integrity of the cathode towards an acidic electrolyte.

© 2022 The Author(s). Published on behalf of The Electrochemical Society by IOP Publishing Limited. This is an open access article distributed under the terms of the Creative Commons Attribution 4.0 License (CC BY, <http://creativecommons.org/licenses/by/4.0/>), which permits unrestricted reuse of the work in any medium, provided the original work is properly cited. [DOI: 10.1149/1945-7111/ac4ab1]



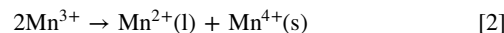
Manuscript submitted October 21, 2021; revised manuscript received December 5, 2021. Published January 21, 2022.

Since the introduction of LiCoO<sub>2</sub> (LCO) by Goodenough et al.<sup>1</sup> four decades ago, research efforts on Li-ion cathode materials have focused on the development of lithiated spinel and layered type transition metal (TM) oxides. The work has been enormously successful considering the widespread application of these oxides in Li-ion batteries of today. Several remaining challenges need however to be addressed. There is a general consensus that battery ageing and failure can largely be attributed to adverse side-reactions involving the TM oxide active materials.<sup>2</sup> Dissolution of the materials constitutes a major challenge since it not only leads to loss of active material, but also accelerates the overall cell ageing. During cycling, the dissolved TMs migrate to and deposit on the graphite anode surface with increased cell impedance and rapidly increasing capacity loss as a result.<sup>3,4</sup> Dissolution is triggered by both thermally- and electrode potential-activated reactions. The most often reported reaction pathway is based on a multi-step process involving electrolyte salt decomposition, hydrogen fluoride (HF) formation, and subsequent oxide corrosion.<sup>5</sup> In line with previous studies,<sup>6,7</sup> we recently observed markedly increased Mn dissolution from TM oxides in electrolytes based on LiPF<sub>6</sub> as compared to LiClO<sub>4</sub>, thus confirming HF as a major cause of dissolution.<sup>5</sup> HF formation from LiPF<sub>6</sub> salt decomposition is commonly claimed to originate from trace water<sup>8,9</sup>



Salt decomposition and TM dissolution are also often reported to be catalyzed by the oxidation of the organic electrolyte components at high potentials.<sup>10,11</sup> For instance, Bloom et al. intentionally introduced possible electrolyte oxidation products: 2,3-butanedione and tetrabutyl ammonium bifluoride as model leaching agents in the electrolyte to study the dissolution process. Tetrabutyl ammonium bifluoride showed a stronger TM leaching degree than 2,3-butanedione, thus evidencing the varying role that certain chemical electrolyte species play during the dissolution of TMs.<sup>12</sup> The electrolyte composition also determines the solubility and stability of soluble TMs, thus possibly also their relative concentration ratios.<sup>7</sup> Most focus has so far been on Mn, because its dissolution is believed to explain the major failure mode behind the highly attractive Li-ion cathode active material LiMn<sub>2</sub>O<sub>4</sub> (LMO). LMO is

based on a spinel crystal structure pertaining to a space group of Fd3m in which a close-packed oxygen array allocates cations in octahedral and tetrahedral sites with equal ratios of Mn<sup>3+</sup> and Mn<sup>4+</sup>.<sup>13,14</sup> Hunter et al.<sup>15</sup> presented an often repeated claim<sup>12,16-19</sup> that dissolution starts with a disproportionation reaction of Mn<sup>3+</sup> according to:



whereby the Mn<sup>2+</sup> species proposedly display higher solubility in the electrolyte. Mn dissolution is however enhanced at higher state-of-charge (SOC) whereby the Mn<sup>4+</sup> oxidation state prevails, thus contradicting a dissolution process predominantly triggered by disproportionation.<sup>20-24</sup> Mn dissolution is furthermore also observed from mixed TM layered LiNi<sub>x</sub>Co<sub>y</sub>Mn<sub>1-x-y</sub>O<sub>2</sub> oxides (NMC) cathodes in which only structural Mn<sup>4+</sup> exist.<sup>3,25</sup> Support for Eq. 2 rather stems from observations of Mn<sup>2+</sup> in the electrolyte and deposited on the anode surface during cycling. The lower oxidation state could alternatively be explained with a process initiated by reductive coupling (TM<sup>4+</sup> + O<sup>2-</sup> → TM<sup>2+</sup> + O.) of TMs at the oxide surface with loosely bound oxygen. Oxygen radicals are highly reactive and known to trigger electrolyte decomposition and formation of leaching agents (such as HF), which in turn assist the dissolution of the remaining undercoordinated surface TM<sup>2+</sup>. In order to counteract Li-ion cathode ageing, thin-film electrode coatings are generally employed. Several metal-oxide, -fluoride and -phosphate based coatings have been observed to suppress TM dissolution.<sup>26-28</sup> Metal-oxides, such as Al<sub>2</sub>O<sub>3</sub>, TiO<sub>2</sub>, ZrO<sub>2</sub>, are reported to better withstand an acidic environment, e.g. involving HF attack.<sup>29,30</sup> Coatings are usually prepared on active materials or electrodes before electrode preparation or cell assembly. Of the most popular coating techniques, such as sol-gel, wet-chemical and atomic layer deposition (ALD), the last technique has proven to be efficient and provide conformal and uniform coatings at relatively low temperatures.<sup>31-34</sup>

Herein, we aim to investigate the thermally-activated TM dissolution mechanism of lithiated and delithiated LMO and NMC in a typical Li-ion electrolyte subjected to hydrolysis and HF formation. Furthermore, we study the role of the most popular coating material, namely Al<sub>2</sub>O<sub>3</sub>, in scavenging HF and suppressing TM dissolution.

## Experimental

**ALD.**—PICOSUN<sup>®</sup> R-200 Standard ALD system was used to deposit Al<sub>2</sub>O<sub>3</sub> on LMO (SEDEMA) and NMC (Heliume Tech) powder. Deposition process was performed at 120 °C. N<sub>2</sub> gas was

<sup>z</sup>E-mail: yonas.tesfamhret@kemi.uu.se; erik.berg@kemi.uu.se

selected as a carrier gas for Trimethylaluminum (TMA) and water precursors. One complete ALD deposition cycle can be described as following: (i) TMA was pulsed for 0.2 s at a flow rate of 15 sccm into the ALD reactor chamber (where the substrate, LMO powder, is situated), followed by a purge with the carrier gas, at a flow rate of 100 sccm. This step was repeated 10 times to achieve a net TMA pulsing time of 2 s. (ii) Reactor was purged with carrier gas for 60 s at flow rate of 600 sccm. (iii) water was pulsed for 0.2 s at a flow rate of 15 sccm followed by purging with carrier gas at a flow rate of 100 sccm. This step was repeated 10 times to achieve a net water pulsing time of 2 s. (iv) Reactor was purged by carrier gas for 60 s at flow rate of 600 sccm. The described steps complete one ALD deposition cycle. LMO and NMC811 samples with 10 ALD deposition cycles of  $\text{Al}_2\text{O}_3$  were prepared and labeled 10CLMO and 10CNMC, respectively.

**Delithiation.**—The pristine and  $\text{Al}_2\text{O}_3$  coated LMO and NMC with the oxidizing agent nitronium tetrafluoroborate ( $\text{NO}_2\text{BF}_4$ ) were introduced to 25 ml of Acetonitrile (Sigma Aldrich) containing 0.2 M  $\text{NO}_2\text{BF}_4$ , in separate 50 ml falcon tubes (VWR). By setting the molar ratio between active material and oxidant to 1:1, the amount of lithium removed was controlled. The LMO and NMC active materials were then stoichiometrically added in the solution and left under stirring for 3 days. The mixture was then washed with acetonitrile in a centrifuge and dried at 60 °C for 12 h in a vacuum oven to remove remaining acetonitrile. The delithiated LMO and NMC powder was then extracted for characterization.

**SEM.**—Scanning electron microscopy (SEM) images and electron dispersive X-ray spectroscopy (EDX) maps were taken using Zeiss/LEO 1550 at 10 kV accelerating voltage.

**Soaking procedure.**—LP40 (1 M  $\text{LiPF}_6$  in 1:1 EC:DEC) electrolyte (medium) was purposely aged to increase the HF concentration, by adding 2000 ppm of water to 30 ml of LP40 (BASF) and resting for 14 days in an Ar-filled glovebox. The electrolyte was initially stirred for 24 h before the long-term storage in PE falcon tube (VWR). The materials of interest for testing were then soaked in the aged electrolyte for 24 h in 2 ml epindorf tubes, before extraction. A corresponding 0.064  $\text{m}^2$  surface area (based on BET measurement) of each pristine sample was soaked in 1.5 ml aged electrolyte. The

soaked materials were removed using syringe filters (0.2  $\mu\text{m}$ , Thermofischer) and the electrolyte was characterized. In order to characterize the alkalinity of the different samples, 200 mg of each sample was immersed in 20 ml Milli-Q water and the increase in pH was measured with SevenCompact Advanced pH Meter Line (Mettler Toledo). For delithiated samples, 50 mg of sample was immersed in 5 ml Milli-Q water. Thus, still sustaining the powder to water ratio of 0.1 mg per 1 ml Milli-Q water. The pH of Milli-Q water was stabilized at 5.8 at first by adding KCl to form 0.001 M KCl (Milli-Q).

**Karl Fischer.**—Coulometric Karl Fischer (KF) titration method was used for the determination water content in the electrolytes pre and post soaking experiments. Metrohm 756 KF Coulometer was used for measurements, where approximately 1 gram of electrolyte was injected into KF reagent solution. The measurement was performed in normal atmospheric conditions. Thus, the samples were equally exposed to the atmosphere (<10 s) before measurement.

**ICP.**—The ICP-OES was calibrated with a 4-point calibration to form a calibration curve. Calibration standards were water based with a known amount of quantified elements ranging from 0.0–10 ppm, Multi-element Calibration Standard (Mettler Toledo). The linear regression created for the HF-probe and ICP-OES insure accurate quantification of HF and TMs, respectively. After soaking, the powders were removed using syringe filters (0.2  $\mu\text{m}$ , Thermofischer). 100  $\mu\text{l}$  of the remaining powderless electrolyte was then sampled for each soaking test and evaporated by heating (250 °C) on a hot plate after transfer to 7.5 ml glass vials (VWR). 5 ml of 90% Milli-Q and 10%  $\text{HNO}_3$  (VWR) was finally added to the glass containers before running ICP measurement.

**Fluoride detector.**—The determination of HF was performed with a  $\text{F}^-$  sensitive ion selective electrode (ISE, Mettler Toledo perfectION combination fluoride electrode). The technique is implemented based on the method development of  $\text{F}^-$  determination in  $\text{LiPF}_6$  electrolytes presented by Strmcnik et al.<sup>35</sup> The  $\text{F}^-$  ISE, which is exclusively sensitive to  $\text{F}^-$ , was calibrated with a series of standards containing a known amount F-ions, prior to measurements. The calibration standards were water based with NaF as a fluoride

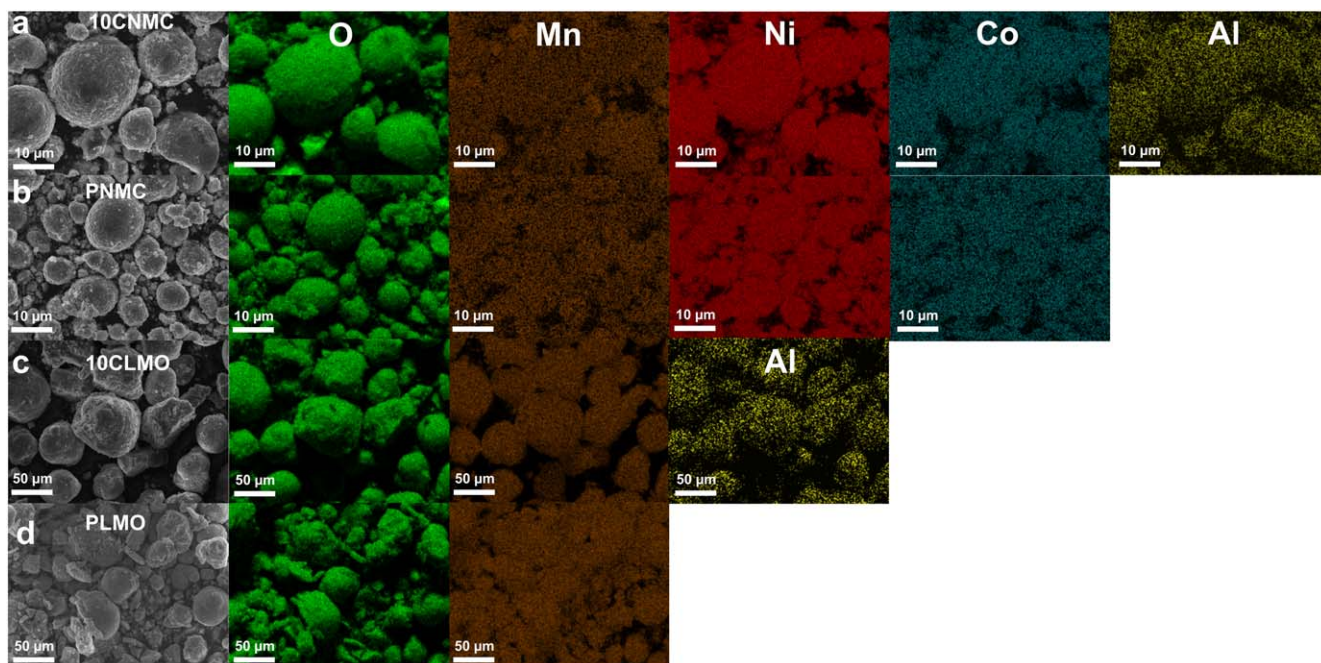


**Figure 1.** SEM images and elemental mappings of O, Ni, Co, Mn and Al in (a) PNMC (b) 10CNMC (c) PLMO and (d) 10CLMO powder.

source. Calibration standards containing  $F^-$  concentration ranging from 0.5–500 ppm were used to formulate a calibration curve, which is subsequently used to determine HF in the electrolytes. A 50:50 vol. % of water and total ion strength adjustment buffer (TISAB) is used as a base, to compensate for charge contribution from impurities.

**BET.**—Nitrogen-gas physisorption (ASAP 2020 analyzer) was employed to determine the Brunauer–Emmett–Teller (BET) surface area of active materials. In combination with ICP quantification of the coating elements present, the  $Al_2O_3$  coating thickness can also be estimated.

## Results and Discussion

First, we characterized the active material powders before (denoted PLMO and PNM) and after (denoted 10CLMO and 10CNMC) ALD coating. The shape and morphology of the powders displayed no apparent structural changes induced by the  $Al_2O_3$  coating (SEM micrographs, Fig. 1). Elemental mapping of Al indicates a homogenous distribution of a very thin (nm)  $Al_2O_3$  coating on both powders. The Ni:Mn:Co molar ratio in both PNM and 10CNMC samples is determined to be 8:1:1, but 0.13 wt% Al is detected in the PNM sample. XPS depth profiling studies of the PNM however revealed that it is presumably a structural additive rather than an already existing oxide coating, which also corroborates with the information provided from the supplier of the powder. The thickness of the  $Al_2O_3$  coating is estimated from the increase in the total amount of Al (quantified with ICP-OES, Table I) on their respective BET surface areas ( $1.86 \text{ m}^2 \text{ g}^{-1}$  and  $0.32 \text{ m}^2 \text{ g}^{-1}$  for PLMO and PNM). The thickness of  $Al_2O_3$  was found to be 0.78 nm and 1.82 nm for 10CLMO and 10CNMC, respectively. The  $Al_2O_3$  coating has been reported to grow at a rate of  $1.1\text{--}1.3 \text{ \AA} \text{ cycle}^{-1}$ , which corresponds to  $1.1\text{--}1.3 \text{ nm}$  after 10 ALD cycles.<sup>36</sup> Deviations from the expected thickness can be explained by the difference in surface area of the PLMO and PNM powders, which in turn can lead to variations in the extent of exposed powder surface to the ALD precursor. The stationary configuration of the ALD reactor employed here is more challenging compared to the fluidized bed ALD reactors commonly employed elsewhere.

In order to delithiate the LMO and NMC powders as mildly as possible without interference from other cell components such as a  $LiPF_6$  based electrolyte or a counter electrode, the active material powders were put in contact with an oxidant  $NO_2BF_4$  dissolved in the highly anodically stable solvent acetonitrile. After the treatment, the residual lithium content was analyzed by ICP-OES and the composition is found to be  $Li_{0.71}Ni_{0.8}Mn_{0.1}Co_{0.1}O_2$  for delithiated PNM and  $Li_{0.47}Ni_{0.8}Mn_{0.1}Co_{0.1}O_2$  for 10CNMC. Likewise, the bulk material composition is found to be  $Li_{0.45}Mn_2O_4$  and  $Li_{0.32}Mn_2O_4$  for delithiated PLMO and 10CLMO, respectively. The ALD coated active materials were thus found to be 13% and 30% more delithiated than the pristine LMO and NMC, respectively. We hypothesize that the coating improves the mechanical integrity of the active materials, e.g. less crack formation during delithiation and 10CNMC was therefore more homogeneously delithiated. The delithiated PNM powder on the other hand would experience more

fractures with the formation of smaller disconnected particles of higher surface areas as a result.

Particles with higher surface area have more contact with the oxidation agent and therefore higher degrees of delithiation compared to larger aggregates of the main PNM powder, which in turn could explain the observed discrepancies above. ICP-OES was used to analyze the  $NO_2BF_4$  containing acetonitrile solution after delithiation to investigate if the delithiation process causes dissolution of TMs (Ni, Co, and Mn) from the cathode structure or Al from the  $Al_2O_3$  coating. Only a small fraction <1% of the active material components was found, likely in the form of small nanoparticles escaping the acetonitrile filtration (<0.2  $\mu\text{m}$  diameter particles may slip through) prior to ICP-OES analysis. Although the measured TM ratios for NMC roughly agree with the overall compositions of the powders, the relative amount of Mn is overrepresented, hence demonstrating that manganese is more susceptible to dissolution during the applied chemical delithiation procedure. Both lithiated and delithiated powders were subsequently exposed to the aged electrolyte. Figure 2 shows the concentrations of HF,  $H_2O$ , and TMs of the electrolyte before (Start) and after contacting the active materials and pure  $Al_2O_3$  powder. Adding 2000 ppm of  $H_2O$  to the LP40 electrolyte stock led during 14 days of storage to the formation of  $\sim 4300$  ppm HF, which is slightly more than the expected  $\sim 4000$  ppm of HF according to Reaction 1. Evidently, not only the salt is affected by the presence of  $H_2O$ , but the solvents are likely also decomposed (e.g. EC is prone to hydrolysis), which in turn leads to more HF. A slight decrease in HF concentration was however recorded each time an HF-containing electrolyte was moved to a fresh container. HF is likely scavenged by the surroundings (e.g. vial walls, pipette tips). This behavior was observed when “Start” solution was transferred to a new vial to form the “Blank” (i.e. no powder contact, Fig. 2) for which about  $\sim 3900$  ppm of HF was recorded after 24 h even without any contact with active materials. A further decrease in HF and a more marked increase in water content is however clearly observed when the electrolytes contact the active materials (Fig. 2). A large fraction of the HF consumed and  $H_2O$  formed can likely be explained by an acid-base reaction in which the acidity of the electrolyte is neutralized by the powders. The alkalinity of the powders was estimated by soaking the powders in Milli-Q water (i.e. deionized water with resistivity > 18.2  $M\Omega \text{ cm}$ ) and recording the change in pH from which the number of released  $OH^-$  per powder surface area was estimated (Fig. 3). As expected, NMC is significantly more alkaline than LMO, which in turn is much more alkaline than the amphoteric  $Al_2O_3$ . NMC contains one more Li per  $TMO_2$  unit than LMO, and is therefore expected to be more alkaline.  $OH^-$  release from the delithiated LMO and NMC powders is also lower in comparison with their lithiated counterparts and thus are expected to be less alkaline. From the  $OH^-$  release (Fig. 3) and HF decrease (Fig. 2) it is also clear that even though the  $Al_2O_3$  coating reduces the respective powder alkalinity, both of the coated LMO and NMC active material powders still maintain significant capacity to neutralize an acid. The remaining relatively high alkalinity of the coated active materials could be due to perseverance of uncoated areas on the active material surface.

Although ALD has been shown to produce excellent and conformal coatings on flat surfaces, maintaining conformality while

**Table I.** Quantitative analysis of the Al in PLMO and  $Al_2O_3$  coated LMO powder by ICP-OES. Presented values are quantified elemental wt%. Al, calculated according to sample size tested.

Active material	BET surface area ( $\text{m}^2 \text{ g}^{-1}$ )	Wt% coated Al	Estimated thickness of $Al_2O_3$ (nm)
PLMO	1.86	—	—
10CLMO	1.92	0.30	0.78
PNM	0.32	—	—
10CNMC	0.42	0.12	1.82
$Al_2O_3$	147,32	—	—

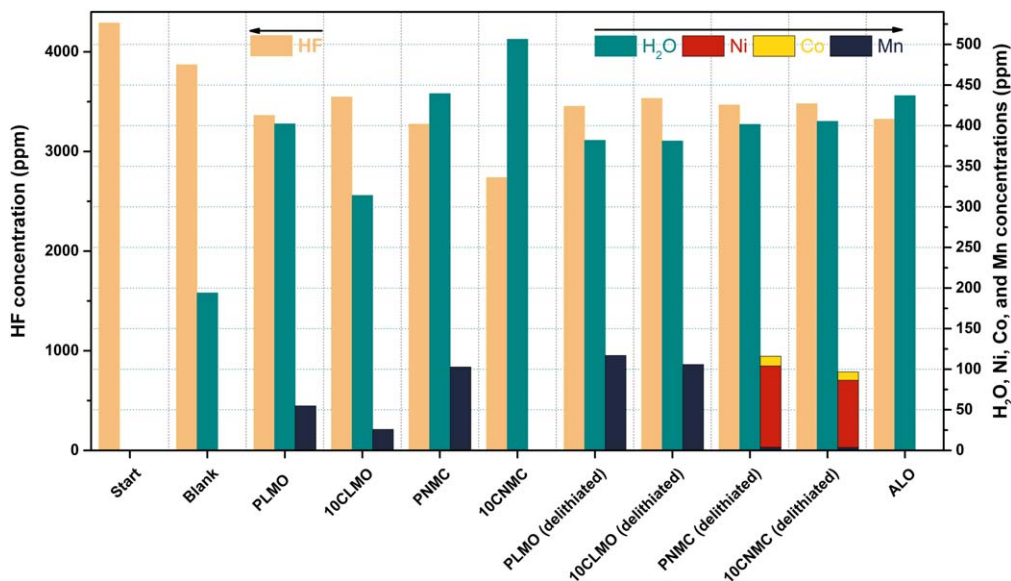
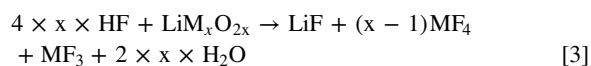


**Figure 2.** Measured HF, H<sub>2</sub>O and TM concentrations of lithiated and delithiated state NMC and LMO, as well as Al<sub>2</sub>O<sub>3</sub> as a reference, after exposure to an aged electrolyte for 24 h. Adding 2000 ppm H<sub>2</sub>O to a stock LP40 electrolyte led to the formation of 4300 ppm HF after 14 days of storage (“Start”). A “Blank” sample is included, in which the “Start” solution was transferred to a fresh vial without any contact with active materials for the duration of the soaking experiment (24 h).

coating porous and powdered materials is challenging.<sup>37</sup> Therefore, it is reasonable to assume that some surface of the active materials remains bare and contributes to a higher alkalinity. Despite the prevalence of the above described acid-base reaction, there is a remaining fraction of HF likely participating in the active material dissolution. The concentration of TMs in the aged electrolyte increased to about 50–100 ppm after contacting the pristine LMO and NMC for 24 h. Despite displaying a lower alkalinity, i.e. a lower propensity to neutralize the HF, the Al<sub>2</sub>O<sub>3</sub> coating clearly decreased the extent of transition metal dissolution from the active materials. Indeed, contacting the pure Al<sub>2</sub>O<sub>3</sub> powder with the aged electrolyte decreased the HF concentration and increased the H<sub>2</sub>O concentration more than when no powder was present (Blank, Fig. 2).

In order to compare the reactivity of the powders, the number of HF consumed, H<sub>2</sub>O and TMs released per surface area of the powders were calculated and presented in Fig. 3. Most importantly, the soaking experiment was designed to expose the same surface area of the powders to the same number of HF. Hence, 6× more NMC powder was soaked in the same volume of aged electrolyte compared to LMO because of the 6x higher surface area of the latter (Table I). With exception of the highly alkaline lithiated NMC powders, all active materials consumed roughly the same moles of HF ( $0.5 \pm 0.1$  mmol m<sup>-2</sup>) and released roughly the same moles of H<sub>2</sub>O ( $0.3 \pm 0.1$  mmol m<sup>-2</sup>). A similar ~2HF/H<sub>2</sub>O ratio is also observed for Al<sub>2</sub>O<sub>3</sub>, although the reaction proceeded to lesser extent due to its lower alkalinity. The higher the alkalinity of the powders the stronger the driving-force for HF to react, which is reflected by larger consumption of HF per surface area of the lithiated NMC. Based on the observed 2HF/H<sub>2</sub>O ratio we may for lithiated active materials propose



and for delithiated active materials



where M is Ni, Co, or Mn and x is either 1 or 2 depending on if we consider NMC or LMO, respectively. For alumina we propose



Indeed, the molar ratios of HF consumed to TM dissolved were found to be in the range 4–10, which evidence the important role of the studied acid-base reaction in governing TM dissolution in Li-ion batteries.

Competing reactions (such as reaction 1) in which both HF and H<sub>2</sub>O may form and/or be consumed render an exact determination of the extent of these acid-base reactions impossible. The moles of TM dissolved correspond to a dissolution of 25%–35% of the total TMs present at the outer surface of the active materials immediately exposed to the electrolyte. TMs present at the surface are most vulnerable to nucleophilic attack by F<sup>-</sup>. The nature and chemical structure of the dissolved TMs were however not further investigated. Both the lithiated and the delithiated active materials released TMs in concentrations of the same order of magnitude when exposed to the aged electrolyte. However, judging from Fig. 3, there is a qualitative trend: (i) uncoated powders released more TMs than coated and (ii) delithiated powders released more TMs than lithiated. Despite a decrease in TM dissolution, the coating is less efficient when the active materials are in the delithiated state. Volume expansion of about 5%–10% for these powders when Li<sup>+</sup> is removed possibly lead to crack formation and exposure of fresh particle surface towards the electrolyte.<sup>14</sup> One reason for the lower concentrations of dissolved Ni, Mn, and Co when the active material is coated could simply be because HF rather attacks the alumina (e.g. according to Eq. 5), which acts as a scavenger for HF.<sup>38</sup> The alumina coating appears to be more effective for NMC compared to LMO. Mn dissolution is almost completely eliminated for NMC in comparison to dissolution being reduced by 53% for LMO. The increased presence of Mn cations on cathodic surface structure has been shown to have a blocking effect on an Al coating-to-dopant transition at the interface between the coating and active material substrate, thus lesser integration.<sup>39</sup> However, in the case of NMC811 (which has a low Mn content of 10%), structural compatibility at the interface between the coating and bulk is expected to be superior compared to LMO, as LMO only comprises Mn as a transition metal. Furthermore, as the thicknesses of Al<sub>2</sub>O<sub>3</sub> suggest, the thicker

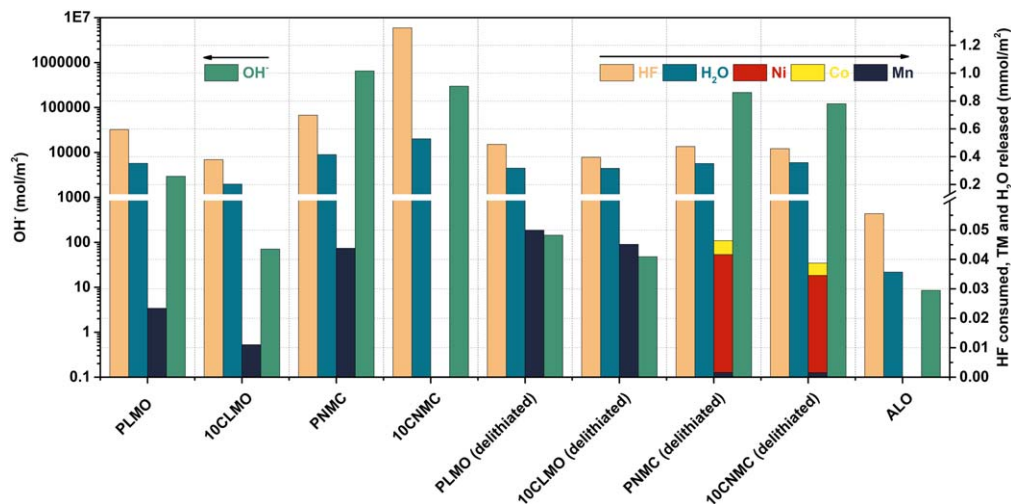


**Figure 3.** HF consumption, TM dissolution and H<sub>2</sub>O formed from soaking experiments of pristine and Al<sub>2</sub>O<sub>3</sub> coated LMO and NMC as well as Al<sub>2</sub>O<sub>3</sub> powder, standardized by surface area. Alkalinity of powders estimated by the OH<sup>-</sup> released according to surface area when soaked in aqueous 0.001 M KCl.

Al<sub>2</sub>O<sub>3</sub> coating on NMC compared to LMO is naturally predicted to provide better protection against the acidic environment provided by the electrolyte. Dissolution of Al was unfortunately not possible to quantify because the electrolyte itself is received and stored in aluminum-based bottles prior to the experiment, which generates a high background signal of Al in the ICP swamping the signal. Another reason for the lower amounts of dissolved TMs for the lithiated active materials could be their lower sensitivity for nucleophilic attack by HF because of the lower acidity of the predominating TM<sup>+3</sup> at the surface. Indeed, lithiated PNMC released almost exclusively Mn, which is the only TM in +IV oxidation state. Furthermore, delithiated LMO (in which only Mn<sup>+4</sup> is found) released twice as much Mn compare to lithiated PLMO (with equal amount of Mn<sup>+3</sup> and Mn<sup>+4</sup>). The popular claim that Mn<sup>+3</sup> is most susceptible TM dissolution due to disproportionation reaction (reaction 2) is therefore implausible. A similar study by Li et al.<sup>40</sup> also found that TM dissolution is more severe in charged LMO than in pristine LMO. When the Li ions are extracted from the structure, oxygen anions hybridize much more strongly with the TMs and as a result are more reactive towards the electrolyte. When HF is present, hydroxyl groups may form on the surface of the active materials, which weakens the bonding between the TM and its surrounding oxygens, eventually resulting in easier TM dissolution from the surface. The removed highly reactive oxygen anions have also been shown to cause electrolyte decomposition and the production of leaching agents (such as HF), which would then aid the dissolution of the remaining undercoordinated surface TMs. Amatucci et al.<sup>40</sup> demonstrated that the amount and which of the TMs dissolve is highly reliant on the ability of the TMs to solvate and form complexes with the degradation products in the electrolyte. For the delithiated NMCs it's no surprise that Ni dissolves to a higher extent, followed by Co and Mn, simply because of the NMC811 composition. The ratio of dissolved TM is however found to be 8:1:0.04 with significantly lower amounts of Mn than expected (Fig. 3). The delithiated powders passed however through a chemical delithiation step prior to the soaking in the aged electrolyte. As mentioned above, the acetonitrile solution with the oxidation agent was however found to be richer in Mn than expected. Unstable Mn at the surface of the NMC powders likely escaped during delithiation, which rendered Ni and Co to be more exposed during soaking in the aged electrolyte. This supports the concept that the presence of the covalent Ni<sup>3+/4+</sup>-O entity has the possibility to withdraw electron density even from Mn-O bonds, making Mn more vulnerable to electrophilic attack by F<sup>-</sup> and dissolution. Hence the overrepresentation of Mn dissolution in PNMC. It is worth pointing out that the Al<sub>2</sub>O<sub>3</sub> coating did not influence the ratio of the dissolved TMs

probably because TM dissolution proceeds at uncoated areas of the active materials.

## Conclusions

HF-activated transition metal dissolution from pristine and coated LMO and NMC powders in lithiated and delithiated states was investigated in an aged Li-ion electrolyte. Ageing of the LiPF<sub>6</sub> based electrolyte was accelerated by including 2000 ppm H<sub>2</sub>O and letting it rest for 14 days, which in turn yielded a HF concentration of 4300 ppm, thus slightly overshooting the expected 2HF consumed per H<sub>2</sub>O formed ratio. Indeed, both HF and H<sub>2</sub>O are known to partake in electrolyte solvent side reactions competing with LiPF<sub>6</sub> salt hydrolysis. Similar 2HF/H<sub>2</sub>O molar ratios were found when the LMO and NMC powders were exposed to the acidic electrolyte. HF is likely neutralized by the alkaline powders in an acid-base reaction forming H<sub>2</sub>O. Powders of higher alkalinity were found to generate more H<sub>2</sub>O when contacting the aged electrolyte. Coating the active materials with Al<sub>2</sub>O<sub>3</sub> generally reduced the alkalinity of the powders and the extent of TM dissolution, especially for the active materials in the lithiated state. Contrary to other reports, reaction between HF and Al<sub>2</sub>O<sub>3</sub> is shown to result in the release of H<sub>2</sub>O, although to a lesser extent than for the LMO and NMC active materials. The lower alkalinity of Al<sub>2</sub>O<sub>3</sub> and its lower propensity to release H<sub>2</sub>O thus dampens the auto-catalytic degradation cycle manifested by combining reaction 1 with reactions 3–5, which may be one of the important roles of active materials coatings for modern Li-ion batteries. Delithiating the LMO and NMC increased the extent of TM dissolution, which is likely due to the higher vulnerability of surface TMs in +IV oxidation state towards HF attack. The lower alkalinity of the delithiated materials also results in lower propensity for neutralizing the acidic surroundings. Although the molar ratios of HF consumed to TM dissolved were found to be in the range 4–10, competing reactions (such as reaction 1) in which both HF and H<sub>2</sub>O may form and/or be consumed render an exact determination of the extent of these acid-base reactions impossible. Nonetheless, these observations challenge the widely accepted disproportionation reaction mechanism for TM dissolution and emphasize the critical role of acid-base reactions in governing TM dissolution in Li-ion batteries.

## Acknowledgments

E.J.B. acknowledges Knut and Alice Wallenberg (KAW) Foundation (Grant 2017.0204) and Swedish Research Council (2016-04069) for financial support. The Swedish Energy Agency via project no. 45518-1 and via StandUp for Energy is acknowledged for the base funding. Dr. Haidong Liu is acknowledged for the

guidance in SEM measurements. Casimir Misiewicz is acknowledged for scientific discussion.

### ORCID

Yonas Tesfamhret <https://orcid.org/0000-0001-9781-5502>

Reza Younesi <https://orcid.org/0000-0003-2538-8104>

Erik J. Berg <https://orcid.org/0000-0001-5653-0383>

### References

1. K. Mizushima, P. C. Jones, P. J. Wiseman, and J. B. Goodenough, *Mater. Res. Bull.*, **15**, 783 (1980).
2. J. P. Pender, G. Jha, D. H. Youn, J. M. Ziegler, I. Andoni, E. J. Choi, A. Heller, B. S. Dunn, P. S. Weiss, R. M. Penner, and C. B. Mullins, *ACS Nano*, **14**, 1243 (2020).
3. C. Zhan, T. Wu, J. Lu, and K. Amine, *Energy Environ. Sci.*, **11**, 243 (2018).
4. T. Nordh, R. Younesi, M. Hahlin, R. F. Duarte, C. Tengstedt, D. Brandell, and K. Edström, *J. Phys. Chem. C*, **120**, 3206 (2016).
5. Y. Tesfamhret, H. Liu, Z. Chai, E. Berg, and R. Younesi, *Chem. Electro. Chem.*, **8**, 1516 (2021).
6. D. R. Gallus, R. Schmitz, R. Wagner, B. Hoffmann, S. Nowak, I. Cekic-Laskovic, R. W. Schmitz, and M. Winter, *Electrochim. Acta*, **134**, 393 (2014).
7. R. Sahore, D. C. O'Hanlon, A. Tornheim, C.-W. Lee, J. C. Garcia, H. Iddir, M. Balasubramanian, and I. Bloom, *J. Electrochem. Soc.*, **167**, 020513 (2020).
8. S. F. Lux, I. T. Lucas, E. Pollak, S. Passerini, M. Winter, and R. Kostecki, *Electrochem. Commun.*, **14**, 47 (2012).
9. A. V. Plakhotnyk, L. Ernst, and R. Schmutzler, *J. Fluor. Chem.*, **126**, 27 (2005).
10. H. Zheng, Q. Sun, G. Liu, X. Song, and V. S. Battaglia, *J. Power Sources*, **207**, 134 (2012).
11. A. Jarry, S. Gottis, Y. S. Yu, J. Roque-Rosell, C. Kim, J. Cabana, J. Kerr, and R. Kostecki, *J. Am. Chem. Soc.*, **137**, 3533 (2015).
12. H. R. Morin, D. G. Graczyk, Y. Tsai, S. Lopykinski, H. Iddir, J. C. Garcia, N. D. Rago, S. Trask, L. Flores, S. Son, Z. Zhang, N. M. Johnson, and I. Bloom, *ACS Appl. Energy Mater.*, **3**, 2565 (2020).
13. S. Dou, *Ionics (Kiel)*, **21**, 3001 (2015).
14. A. Van Der Ven, C. Marianetti, D. Morgan, and G. Ceder, *Solid State Ionics*, **135**, 21 (2000).
15. J. C. Hunter, *J. Solid State Chem.*, **39**, 142 (1981).
16. R. J. Gummow, A. de Kock, and M. M. Thackeray, *Solid State Ionics*, **69**, 59 (1994).
17. D. H. Jang, Y. J. Shin, and S. M. Oh, *J. Electrochem. Soc.*, **143**, 2204 (1996).
18. B. Aktekin, M. J. Lacey, T. Nordh, R. Younesi, C. Tengstedt, W. Zipprich, D. Brandell, and K. Edström, *J. Phys. Chem. C*, **122**, 11234 (2018).
19. M. Wohlfahrt-Mehrens, C. Vogler, and J. Garche, *J. Power Sources* (Elsevier, Amsterdam) **127**, p. 58 (2004).
20. A. Du Pasquier, A. Blyr, P. Courjal, D. Larcher, G. Amatucci, B. Gérard, and J. M. Tarascon, *J. Electrochem. Soc.*, **146**, 428 (1999).
21. G. G. Amatucci, A. Blyr, C. Sigala, P. Alfonse, and J. M. Tarascon, *Solid State Ionics*, **104**, 13 (1997).
22. K. Nishimura, T. Douzono, M. Kasai, H. Andou, Y. Muranaka, and Y. Kozono, *J. Power Sources*, **81–82**, 420 (1999).
23. A. Antonini, C. Bellitto, M. Pasquali, and G. Pistoia, *J. Electrochem. Soc.*, **145**, 2726 (1998).
24. L. Cai, Y. Dai, M. Nicholson, R. E. White, K. Jagannathan, and G. Bhatia, *J. Power Sources*, **221**, 191 (2013).
25. S. J. Wachs, C. Behling, J. Ranninger, J. Möller, K. J. J. Mayrhofer, and B. B. Berkes, *ACS Appl. Mater. Interfaces*, **13**, 33075 (2021).
26. F. Mattelaer, P. M. Vereecken, J. Dendooven, and C. Detavernier, *Adv. Mater. Interfaces*, **4**, 1601237 (2017).
27. Z. Chen, Y. Qin, K. Amine, and Y. K. Sun, *J. Mater. Chem.*, **20**, 7606 (2010).
28. X. Xiao, P. Lu, and D. Ahn, *Adv. Mater.*, **23**, 3911 (2011).
29. J. Cho, Y. J. Kim, T. J. Kim, and B. Park, *Angew. Chemie - Int. Ed.*, **40**, 3367 (2001).
30. I. D. Scott, Y. S. Jung, A. S. Cavanagh, Y. Yan, A. C. Dillon, S. M. George, and S. H. Lee, *Nano Lett.*, **11**, 414 (2011).
31. Q. Qiu, X. Huang, Y. Chen, Y. Tan, and W. Lv, *Ceram. Int.*, **40**, 10511 (2014).
32. A. Zhou, Q. Liu, Y. Wang, W. Wang, X. Yao, W. Hu, L. Zhang, X. Yu, J. Li, and H. Li, *J. Mater. Chem. A*, **5**, 24361 (2017).
33. Y. Su, S. Cui, Z. Zhuo, W. Yang, X. Wang, and F. Pan, *ACS Appl. Mater. Interfaces*, **7**, 25105 (2015).
34. R. L. Patel, J. Park, and X. Liang, *RSC Adv.*, **6**, 98768 (2016).
35. D. Strmcnik, I. E. Castelli, J. G. Connell, D. Haering, M. Zorko, P. Martins, P. P. Lopes, B. Genorio, T. Østergaard, H. A. Gasteiger, F. Maglia, B. K. Antonopoulos, V. R. Stamenkovic, J. Rossmeisl, and N. M. Markovic, *Nat. Catal.*, **1**, 255 (2018).
36. L. Chen, R. E. Warburton, K. S. Chen, J. A. Libera, C. Johnson, Z. Yang, M. C. Hersam, J. P. Greeley, and J. W. Elam, *Chem*, **4**, 2418 (2018).
37. J. S. Daubert, R. Wang, J. S. Ovental, H. F. Barton, R. Rajagopalan, V. Augustyn, and G. N. Parsons, *J. Mater. Chem. A*, **5**, 13086 (2017).
38. X. Li, J. Liu, X. Meng, Y. Tang, M. N. Banis, J. Yang, Y. Hu, R. Li, M. Cai, and X. Sun, *J. Power Sources*, **247**, 57 (2014).
39. B. Han, B. Key, S. H. Lapidus, J. C. Garcia, H. Iddir, J. T. Vaughey, and F. Dogan, *ACS Appl. Mater. Interfaces*, **9**, 41291 (2017).
40. N. V. Faenza, Z. W. Lebens-Higgins, P. Mukherjee, S. Sallis, N. Pereira, F. Badway, A. Halajko, G. Ceder, F. Cosandey, L. F. J. Piper, and G. G. Amatucci, *Langmuir*, **33**, 9333 (2017).